Astron. Astrophys. 253, 389–402 (1992)

ASTRONOMY AND ASTROPHYSICS

A magnitude, colour, and proper-motion probe of the Galaxy at an intermediate galactic latitude ⋆

O. Bienaymé [1], V. Mohan [2], M. Crézé [3], S. Considère [1], and A.C. Robin [1,3]

[1] Observatoire de Besançon, 41 bis Av. de l'Observatoire, BP 1615, F-25010 Besançon Cedex, France
[2] Uttar Pradesh State Observatory, Manora Peak, Nainital, 233129, India
[3] Observatoire de Strasbourg, CNRS URA 1280, 11 rue de l'Université, F-67000 Strasbourg, France

Received July 1, accepted August 21, 1991

Abstract. A sample survey is being conducted in *UBV* photometry and proper motions as part of an investigation of galactic structure and evolution. In the present paper we discuss the observational results in a restricted field (1.78 square degree) at intermediate galactic latitude in the direction of the globular cluster M5. The resulting catalogue includes 1180 stars, it is complete down to $B=18$, $V=17.4$, and $U=18$. The plate material has been obtained at the CERGA Schmidt telescope between 1984 and 1990. Glass copies of the Palomar Observatory Sky Survey (POSS, 1955) have been used as first epoch for proper motions. Plates have been digitized using the MAMA machine at the Observatoire de Paris.

The accuracy of relative proper motions is better than $3\,\mathrm{mas\,yr^{-1}}$ for stars brighter than $V=16.5$. The photometric accuracy ranges between 0.08 and 0.10 in the three bands. We discuss the main points relevant to astrometric accuracy: digitization, efficiency of centering algorithms, plate to plate transform using orthogonal polynomials and effect of unmodelled distortions.

Key words: astrometry – photometry – kinematics and dynamic of the Galaxy – structure of the Galaxy – stellar content of the Galaxy

1. Introduction

Currently accepted ideas concerning the structure and evolution of stellar populations in our Galaxy are mainly based on detailed observations of stars in the close solar neighbourhood. Faint star counts have long been advocated only to get an overview of the large scale features (Van Rhijn 1965; McCuskey 1965; Bok & Basinski 1964). Apart from the pioneering work of the Basel Halo-Disc program (Becker 1965), only recently should the modern digitization and processing facilities open the way to getting medium accuracy photometry for complete faint star probes in large selected fields (Chiu 1980; Sandage 1987; Gilmore & Wyse 1985; Mohan & Crézé 1987), thus giving access to the properties of star samples out of the solar neighbourhood. In some cases (Chiu 1980; Spaenhauer 1989; Reid 1990) the measurements include both photometry and proper motions.

The raw observational data which can be obtained for many faint stars do not allow the derivation of intrinsic stellar parameters such as distance, mass, age, space velocity, chemical composition, evolutionary stage, interstellar extinction of individual stars. However, some information relevant to the distribution of these quantities is reflected in the n-dimensional distribution of observables: proper motions depend on distances and space velocities which are themselves the result of star formation and dynamical processes. Magnitudes and colours are also connected to ages and star formation processes through the history of star formation and stellar evolution. Connecting observable distributions to the main processes they come from is basically a multivariate problem for which we have developed at the Observatoire de Besançon both a synthetic approach of galaxy modelling hereafter referred to as Besançon model (Robin & Crézé 1986; Bienaymé et al. 1987) and a multivariate sample survey plan including complete samples of *UBV* photometry and proper motions in a set of galactic fields. It is essential for the synthetic interpretation of such data that calibration problems and residual sources of systematic errors remain under control. The photometric aspects have been presented elsewhere (Mohan & Crézé 1987).

In the present paper we give the results of a first sample including photometry and proper motions together with a discussion of the technical aspects of the astrometric measurements. A photometric (*UBV*) and astrometric (relative proper motions) survey is obtained in a 1.78 square degree field centered on $l=3°$, $b=47°$, near the globular cluster M5. The resulting catalogue contains 1180 stars, and is complete down to $B=18$, $V=17.4$, $U=18$.

Send offprint requests to: O. Bienaymé

⋆ Based on observations at Nainital (India) and at CFH (Hawaii), on photographic plates obtained with the CERGA Schmidt telescope, and on glass copies from the first epoch POSS. Digitizations made with the MAMA measuring machine. MAMA is developed and operated by INSU (Institut National des Sciences de l'Univers).

Table 1. Plate material

Plate number	Emulsion + filter	Colour	Exposure time (s)	Night
CERGA Schmidt plates				
1036	IIaO + GG 385	*B*	780	26/4/84
1037	IIaO + GG 385	*B*	812	26/4/84
1523	IIaD + GG 495	*V*	2700	12/5/86
1512	IIaO + UGI	*U*	7200	14/4/86
1543	IIaD + GG 495	*V*	2700	6/6/86
2446	IIaO + UGI	*U*	7200	4/3/90
POSS copy				
PO 1402	103a-E + red Plexiglass		3000	19/4/55

2. Plate material and measurements

The photographic material used in this project is described in Table 1. Plates were exposed at the CERGA 1 meter Schmidt telescope between 1984 and 1990. The filter/emulsion combinations of the 6 CERGA plates give approximately the Johnson *U*, *B*, and *V* bands. A glass copy of the Palomar Observatory Sky Survey (POSS) is used as a first epoch for proper motions thus providing a 31 year time baseline with the CERGA plate number 1523 as the second epoch. All plate measurements have been performed with the digitizing machine at the Observatoire de Paris (MAMA) which is optimized for astrometric performance. The resulting accuracy at least for strictly differential proper motions supports the conclusion that plates from different telescopes and even glass copies can be successfully used without major degradation of the astrometric results.

About 60 photoelectric standards have been used from various authors and from new observations (Appendix A). Magnitudes are determined on CERGA plates over about 64 cm^2 (2 square degrees) which overlap two different POSS plates. Only one POSS plate and the CERGA plate number 1523 have been scanned for astrometry. The final catalogue covers 1.78 square degrees.

For the photometry CERGA plates are digitized with a 10 μm pixel. The digitized image is stored and processed on line giving a catalogue of detected objects at a given threshold above the background. The integrated density above the threshold is used as a magnitude index.

Plates measured for astrometric purposes are also digitized with a 10 μm pixel. Digitized images are stored on magnetic tapes and reprocessed off line for star detection and centering. The centering accuracy turns out to be about 0.5 μm on either coordinates. No evidence is found that using a smaller pixel size would improve this result.

Our direct tests of the astrometric capability of this program do confirm that this half micron limit is presently the state of the art of the MAMA machine (see also Berger et al. 1991). The repeatability over 24 h is of the order of 0.5 μm. The coordinates given by the machine have been controlled using a Nanomask® plate covered by large dots. Scans with different plate orientations over a $12 \times 12\,cm^2$ area do provide an external calibration of the MAMA reference system: dot positions are again obtained with an accuracy of 0.5 μm. More extensive tests performed by the MAMA team, show that this accuracy is achieved over the whole scanning table.

Table 2. Standard deviation of magnitudes from plate-plate comparison

m_B	σ_V	σ_B	σ_U
12.5	0.03	0.03	0.05
13.5	0.03	0.03	0.06
14.5	0.03	0.03	0.06
15.5	0.04	0.04	0.07
16.5	0.05	0.05	0.08
17.5	0.06	0.05	0.09

3. Photographic photometry

3.1. Image processing

During the digitization, on-line routines filter images and extract an object catalogue with positions and density measurements. The plate-to-plate cross-identification helps the rejection of spurious detections while the performance of the acquisition-reduction can be estimated by density comparison of same stars between similar plates. The plate-plate dispersion is 0.03 mag r.m.s. for the brightest stars (Table 2). This contribution is small compared to the scatter of stars ($0^m.09$–$0^m.10$) about the calibration curve. The star – non-stellar object separation is performed by plotting the integrated density versus area diagram (non-stellar objects may be galaxies as well as overlapping stars). From this diagram we have defined for $V > 15$ the probability for an object to be a star. Then 88 non-stellar objects are detected on 2 square degrees down to $V = 17.4$. On deepest plates (number 1523 and 1543), separation remains well defined down to the completness limit of the final catalogue ($V = 17.4$).

3.2. Detection completeness

Some loss of completeness is likely to be due to image overlap. To estimate this effect, we investigate the statistics of the distance r from each star to its closest neighbour. Stars are sorted in increasing order of r. Let $N(r)$ be the rank of a star. If stars were randomly and uniformly distributed over the field, the cumulative

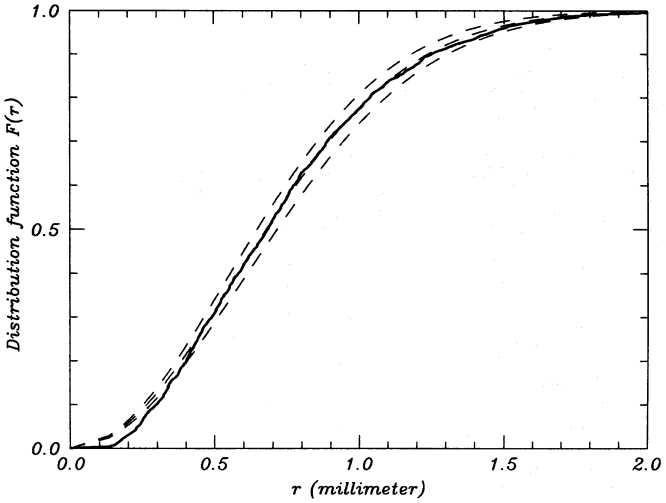

Fig. 1. Distribution function of distances of the nearest neighbour observed (solid line) and theoretical (dashed) in random uniform distributions with various mean densities ($\varrho = 1.35$, 1.50, 1.65). The discrepancy at low r's is produced by undetected overlapping images, the resulting uncompleteness is about 0.8%

frequency function of the distance to the nearest neighbour would be given by (1)

$$F(r) = 1 - \exp(-\varrho \pi r^2), \quad (1)$$

where ϱ is the mean star density. Let N_{tot} be the number of stars in the catalogue, since $N(\boldsymbol{r})$ is the number of stars with a neighbour closer than $\boldsymbol{r}$, $N(\boldsymbol{r})/N_{tot}$ is approximately the cumulative frequency function. In Fig. 1, we plot the measured distribution function $N(\boldsymbol{r})/N_{tot}$ and three functions given by Eq. (1) for three ϱ values. We find that the density of the catalogue is 1.50 stars per square millimeter on CERGA plates. However we can see differences between the measured and expected functions for small r value. The completeness is clearly lost below 450 μm: stars with separations smaller than 200 μm (14″) are merged. The completeness can be determined by integrating the difference between the measured function and the expected one for $\varrho = 1.50$ star mm^{-2}. The completeness turns out to be better than 99%.

3.3. *Calibration curve*

Photometric sequences from various authors have been used in the calibration process. Photoelectric or CCD *UBV* magnitudes used in the calibration can be found in Arp (1962), Richer & Fahlman (1987), Stetson & Harris (1988), and in Mohan (1987). In addition, some new observations obtained with the CFH 3.6 m telescope are used. *UBV* magnitudes in the Johnson system are given together with coordinates for identification purposes in Appendix A, Table 1. Most faint standards are concentrated near the globular cluster M5. According to Arp (1962) his photometry is not affected by the background light from M5. The different data sources have been compared and checked for consistency. Bright standards have been photoelectrically measured by one of the authors (V. Mohan) with the 1 m telescope of the Uttar Pradesh State Observatory at Nainital (India). These brightest stars are spread over the field of our survey and are used to check for geometrical variations of the sensitivity over the plates.

Finally 51 stars in V, 55 in B, and 41 in U are used in the calibration (for which photometric magnitudes exist and density measurements on plates are accurate). *UBV* standard colours converted into photographic instrumental colours (u, b, v) using Eqs. (2)–(4) (valid for the emulsion-filter combination given in Table 1). These equations have been previously determined by calibrating the CERGA Schmidt telescope (Mohan & Crézé 1987) using a large number of photoelectric sequences in clusters with a large spread in colour.

$$v_{inst} = V_{Johnson} - 0.14\,(B-V), \quad (2)$$

$$b_{inst} = B_{Johnson} - 0.16\,(B-V), \quad (3)$$

$$u_{inst} = U_{Johnson} - 0.16\,(B-V) + 0.10\,(U-B). \quad (4)$$

Calibration curves are obtained by fitting a third degree polynomial to the integrated density versus magnitude plot (Fig. 2). Standards giving residuals greater than three times the rms have been rejected. For all plates the rms magnitude scatter ranges from 0.08 to 0.10 in the magnitude range 11 through 18. Higher order calibration polynomials would not reduce significantly the residuals and might result in systematic errors. Figure 3 shows the

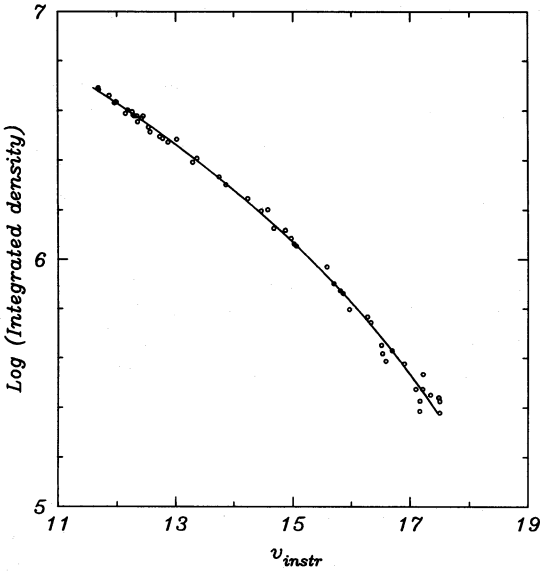

Fig. 2. Calibration curve for CERGA 1543 plate fitting. Instrumental magnitude v versus logarithm of the integrated density measured on plates

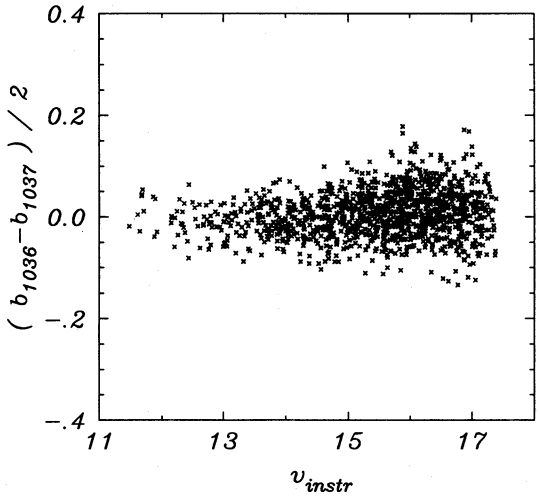

Fig. 3. Half differences of instrumental b magnitudes between CERGA plates 1036 and 1037 versus magnitude. The rms of ordinates is a measure of internal errors (see Table 2)

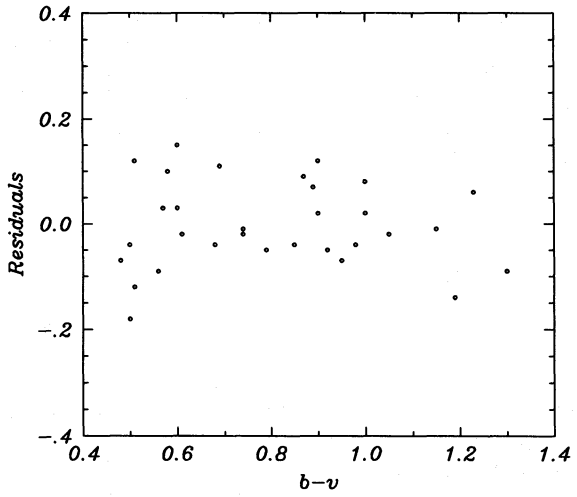

Fig. 4. Residuals of standards to the calibration curve versus instrumental colour $b-v$ (stars with $v<15$). Similar diagrams based on more standards are given in Mohan & Crézé (1987) to validate the colour Eqs. (2)–(4)

plate-to-plate half-differences of b magnitudes which are a measure of internal errors as summarized in Table 2. So residual deviations from the calibration curve remain larger than the plate-to-plate density deviations.

Hence we obtain a first determination of u, b, and v magnitudes defined as the mean of the magnitudes measured on each plate pair.

Residuals from the best-fit polynomial calibration are plotted in Fig. 4 as a function of colours for 31 standards brighter than $V=15$ showing no significant colour effect. Colour Eqs. (2)–(4) (from Mohan & Crézé 1987) are more accurately defined than just using the existing standards in our field.

3.4. *Flat fielding*

The plate-to-plate magnitude comparison shows geometrical variations or systematic field effects due to sensitivity variation according to position (for a general treatment see Mohan & Crézé 1987). The maximum geometrical variations across the field is found to be only 0.025 on v and b plates. In u the maximum discrepancy is 0.06 comparable to the random errors. Plate-to-plate comparisons are not sufficient to measure geometrical variations due to non-uniform transmission of the telescope and filters; standards spread over the whole field are needed for this purpose.

Another way in which this flat fielding correction can be estimated is if the average colour of stars in any subfield is position independent. This is true at least over 2 square degrees and since no differential absorption effects are expected in this intermediate galactic latitude field. Both methods yield the same geometrical terms, although the second one is more accurate. The measured variations of the average $u-b$ or $b-v$ between subfields (respectively ± 0.15 and ± 0.06 maximum variation) are then entirely attributed to geometrical bias. Using a linear fit in x and y coordinates, we have corrected the $u-b$ and $b-v$ indices so that their mean values for each subfield remain constant over the whole field. This correction shifts indices by an unknown constant which is determined using the bright standards. The $U-B$, $B-V$ diagrams for stars brighter than $V=16$ before and after geometrical corrections have been applied (Fig. 5a, b) shows the improvement due to flat fielding. This correction confines the data along the main sequence.

3.5. *Photometric catalogue*

The instrumental photographic magnitudes are converted to the Johnson system using Eqs. (2) through (4). Figure 5b shows the resulting $U-B$, $B-V$ diagram.

A striking feature of the diagram is the deviation of the data points from the main sequence (solid line). This fact could be related to unidentified systematics errors with the U photographic calibration. However the diagram is very similar to those obtained by Yoshii et al. (1987) in UBV or Fenkhart & Karaali (1990) in RGU in the same field. Most authors attribute this deviation to the $U-B$ excess of halo stars.

Figure 6 shows v magnitude counts from both plates; v counts appear to be complete at least to $v=17.4$. From similar histograms, the completeness limits of the ubv catalogue are found to

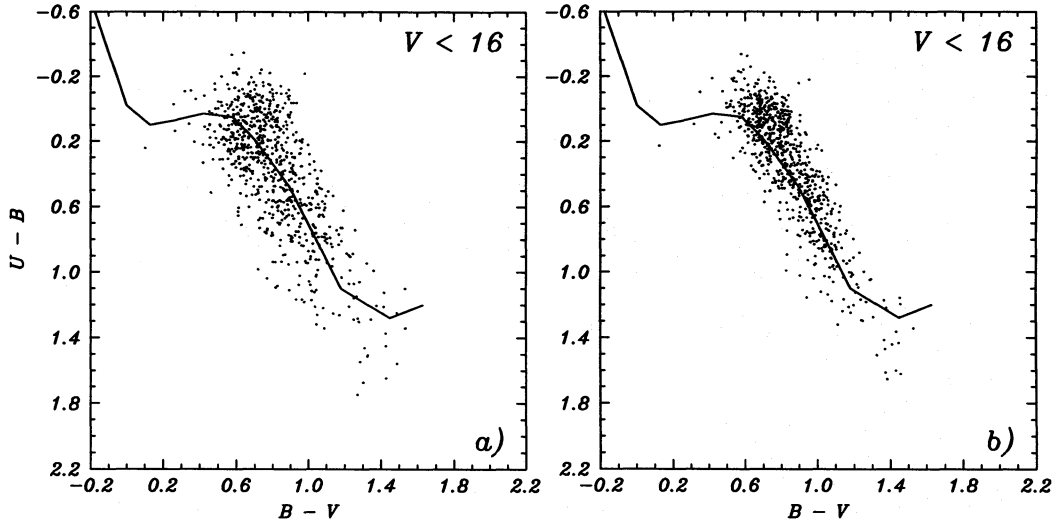

Fig. 5a and b. $U-B$ versus $B-V$ diagram are converted to the standard system for stars with $V<16$. The full line locates the main sequence. **a** Data without geometrical correction. **b** Dispersion of data is lowered after geometrical corrections

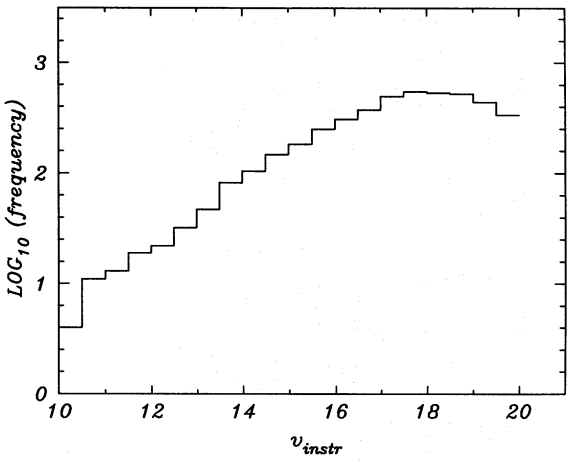

Fig. 6. Histogram of instrumental v counts. From this diagram, completness turns out to be lost beyond $v = 17.4$

be $u < 18$, $b < 18$, and $v < 17.4$. Figures 7 show $b-v$ and $u-b$ histograms for three magnitude intervals with the Besançon model predictions (see Sect. 5). Red stars are lost for histograms with $V > 16$ because of b magnitude cut-offs. A good agreement is obtained with $b-v$ data, while the above quoted deviation of the $u-b$ data is still clearly visible.

4. Photographic astrometry

The present astrometric analysis has been conceived as purely differential. The displacement of each stellar image is measured relative to the framework defined by all stars in the field. Then errors result from the inaccuracy of the centering process (Sect. 4.1) combined with the inaccuracy of the plate-plate transform (Sect. 4.2.2). The former contribution mainly reflects the performances of the measuring machine and the centering algorithms and to lesser extent the image quality (Sect. 4.1.3). The latter contribution can be substantially reduced as compared with classical astrometry since it is equivalent to using hundreds of reference stars per square degree. Systematic effects such as colour effects or magnitude effects may still be present (Sect. 4.2.3) although the differential refraction is found to play a negligible role (Sect. 4.1.4).

4.1. Centering

4.1.1. General tests on centering algorithms

The performances of a number of centering algorithms have been intensively tested (Bienaymé et al. 1988). The first tests are based on synthesized images adding a poissonian background to gaussian stellar profiles. As long as the signal-to-noise ratio is high enough and the centering window is suitably tuned to the size of the stellar profile, all algorithms give similar results in agreement with the optimal accuracy deduced from statistical considerations.

Tests in more realistic conditions have been performed using a set of 120 CCD frames. CCD images do provide an intermediate bench for testing algorithms in more complex situations and the noise statistics can be modeled far better than in the case of photography. In those more realistic conditions, the algorithms are no longer equivalent. In contradiction to the claims by Stone (1989), the gravity center methods, however modified, do not reach the optimal accuracy. They are extremely sensitive to blended images and plate defects.

4.1.2. Centering on Schmidt plates

Due to strongly non-linear effects, we do not have a good statistical model relating the properties of images on photographic

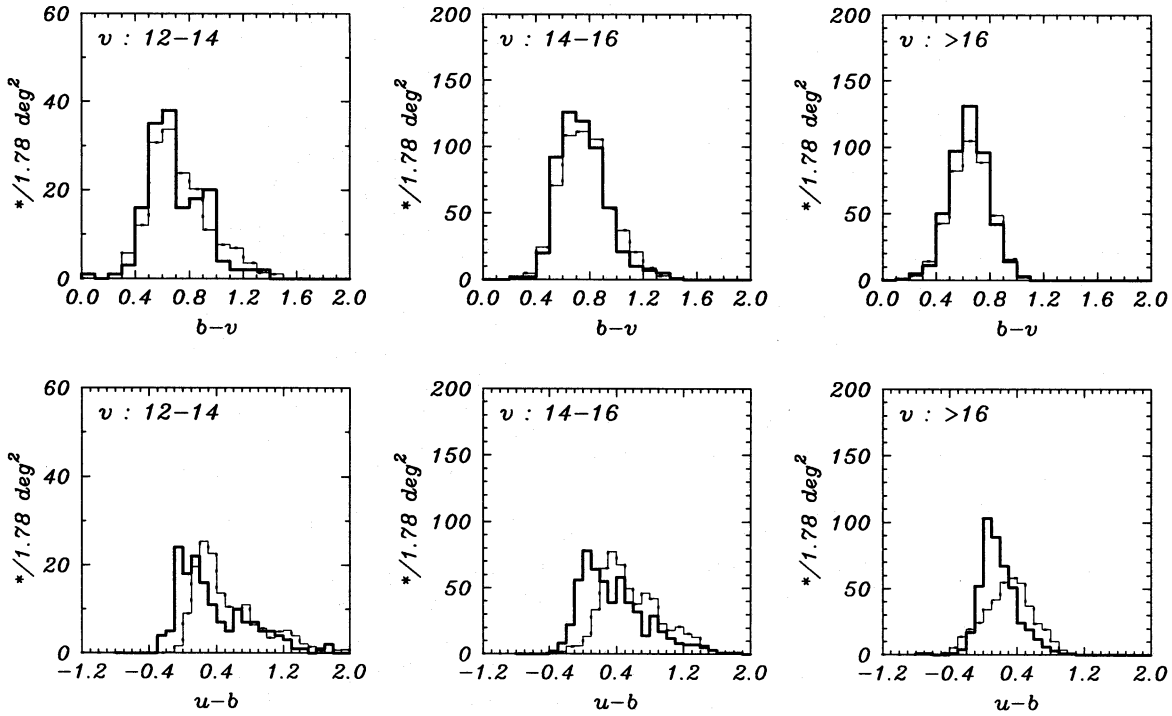

Fig. 7. Histogram of $b-v$ and $u-b$ instrumental indices for three magnitude intervals. Data (solid lines) and model prediction (thin dotted lines)

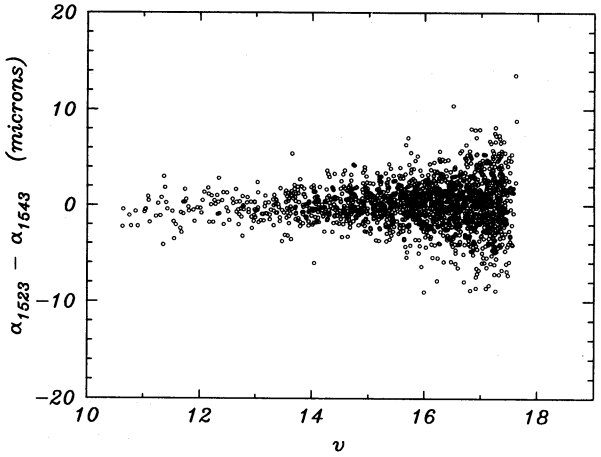

Fig. 8. Plate-plate comparison with null proper motions. Right ascension proper motions in microns are plotted versus v magnitude. The time baseline (plates 1523 and 1543) being less than 1 month, the dispersion reflects only the centering accuracy (gravity center method)

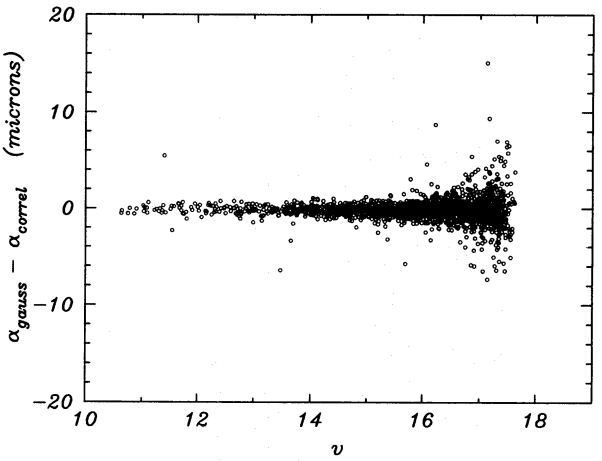

Fig. 9. Algorithm comparison on a single plate (1523). Comparison along one coordinate between autocorrelation centers and gaussian fitting centers

plates to signal properties. So, only empirical investigations can help optimizing centering algorithms. The present investigation is based on deriving proper motion solutions from positions obtained from two different plates exposed at the same epoch (zero proper motions) or from comparing positions obtained on the same plate with different algorithms. Three families of algorithms have been tested:

- gravity center method
- 1-dimensional gaussian profile fitting
- 2-dimensional correlation method

The methods have been described in Bienaymé et al. (1988).

The test bench is provided by two CERGA plates (namely plates 1523 and 1543) with epochs differing by less than four weeks. The proper motion statistics resulting from the gravity center method being applied to either plate is illustrated in Fig. 8. Standard deviations as a function of magnitude is given in Table 3 column 3. They range from 1.5 μm at magnitude 11 to 3.2 μm at magnitude 17.

Now if the autocorrelation centers obtained on plate 1523 are substituted for gravity-center ones in the proper motion solution, we get the standard deviations indicated in column 4 which are 10% to 20% smaller. So the gravity center centering is far from achieving the minimum variance over the whole magnitude range.

Then if autocorrelation centers are compared to 1-D gaussian profile fitting centers on the same plate (Fig. 9 and column 8 in Table 3), the disagreement between the two estimates based on basically different estimators is too small to expect any further substantial improvement at least at acceptable level of sophistication and cost of the algorithms.

There is however a remote tail in the distribution of differences between the results of the last two algorithms: in a very limited number of cases, the disagreement is so large that it was necessary to go back to images and see what each center actually means. All those cases turn out to be related to blends either between stellar images or between stellar images and plate defects. Whenever the image shows a real center which algorithms should be expected to find out, the autocorrelation method does provide the best estimate of the real center. Thus among the two methods providing in general the most accurate centering, the autocorrelation proves more robust to image anomalies. Our final proper motion solution is based on this algorithm.

Table 3. Accuracy in μm of centering methods and plate comparisons. Col. 1: magnitude bins. Col. 2: number of comparison stars. Col. 3: rms proper motion from gravity center positions between plate 1523 and 1543 (same epoch). Col. 4: same as col. 3 between gravity center method on plate 1543 and from the autocorrelation method on plate 1523. Cols. 5 and 6: rms positional accuracy from the gravity center method (5) and the autocorrelation method (6) deduced from columns 3 and 4. Col. 7: rms difference between gravity and correlation centers on the same plate 1523. Col. 8: rms difference between gaussian fit and correlation centers on the same plate 1523

1	2	3	4	5	6	7	8
11–12	33	1.46	1.38	1.03	0.92	1.03	1.10
12–13	52	1.16	1.13	0.82	0.78	0.66	0.47
13–14	110	1.51	1.39	1.07	0.89	0.79	0.78
14–15	220	1.46	1.24	1.03	0.69	0.89	0.48
15–16	377	1.81	1.56	1.28	0.89	1.19	0.69
16–16.5	282	2.21	1.92	1.56	1.12	1.61	0.98
16.5–17	330	2.62	2.31	1.85	1.38	1.75	2.32
17–17.5	455	3.21	3.08	2.27	2.08	2.45	2.80

4.1.3. Non-circular images

The centering accuracy strongly depends on the plate quality. Two plates with strongly elongated stellar images have been used to test this effect. Proper motions between these plates exposed during the same month should in principle be negligible and magnitude independent. The average proper motion of bright stars ($V = 14$) relative to the faint ($V = 18$) is 5 μm (0.″3). This magnitude effect can be explained by the fact that density peaks of stellar images are obviously off-centered with respect to the wings. Faint star centers are then found near the maximum density while for bright stars the wings do contribute significantly. The plates used in this specific test are unusually bad and should not be used for astrometric purposes.

On the plates used in our M 5 survey, images do not show any sizable departure from circularity. The magnitude bias from

Table 4. Average proper motions on x and y coordinate (columns 3, 4) in μm from 1523 and 1543 plates. The scale is $0''.07\,\mu m^{-1}$. Column 1 and 2 as in Table 3

1 V	2	3 μ_x	4 μ_y
11–12	33	−0.6	0.0
12–13	52	−0.2	0.1
13–14	110	−0.2	0.2
14–15	220	0.1	0.3
15–16	377	0.2	0.2
16–16.5	282	0.0	0.4
16.5–17	330	0.1	0.1
17–17.5	455	0.2	0.0

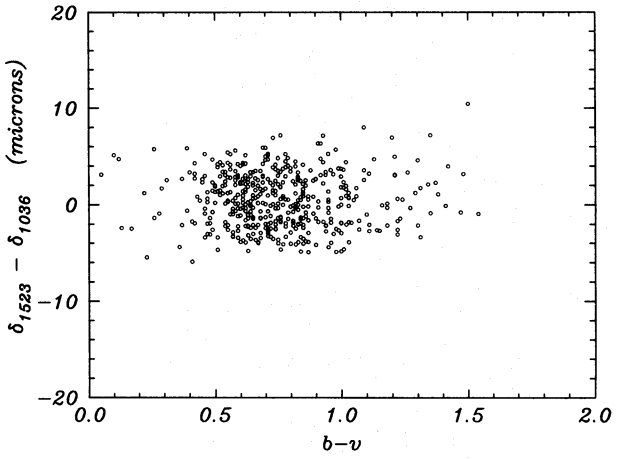

Fig. 10. Delta proper motions in microns between V plate 1523 and B plate 1036 for stars with $v<15$ (one year time baseline). There is no evidence for any significant colour equation

1523–1543 plate comparison is given in Table 4 (cols. 3, 4). It is negligible (smaller than 0.4 μm or $0''.025$) except for the brightest stars.

4.1.4. Atmospheric refraction

Additional systematic errors are expected to result from the differential atmospheric refraction which may create a colour term in proper motions between plates taken at different zenith angles. This effect has been estimated using equations given by Murray & Corben (1979) and Kovalevsky (1990). Since our astrometric plates are taken at small zenith angles (30° and 40°), this effect is expected to be small. The maximum effect on CERGA plate 1523 is found to be at a 0.2 μm level between the bluest and the reddest stars. We have also made a direct comparison between the V 1523 plate and the B 1036 plate: Fig. 10 shows proper motions (with a 2 yr time baseline) versus $b-v$ indices for bright stars with $v<15$. No systematic effect can be measured. From Fig. 10 the colour term in proper motions is found to be less than 0.4 μm per unit in $B-V$ (slope: 0.0 ± 0.4). Since the chromatic effect is about two times larger with B filters than with V filters (in the present situation), it can be neglected for the present astrometric reduction based on V plates, so finally no correction has been applied.

4.2. *Proper motion solution*

4.2.1. Cross-identification

Following a classical cross-identification scheme, a first approximate plate-plate transform is computed using a few bright stars. Then centers from one plate are transformed into the coordinate system of the other one and counterpart candidates are searched for within a 250 μm radius (16″) around each projected center. The nearest candidate within this circle is adopted as counterpart and magnitudes are checked for consistency. Identification errors are found to be rare. However, since the POSS plate is far deeper than the CERGA one, blends between neighbouring stars are more frequent generating a few identification errors most of which can be easily corrected. A dozen suspect pairings remain in the catalogue. From the restricted size of the search window, no proper motions larger than $0''.4\,yr^{-1}$ can be detected.

4.2.2. Plate transform

A mathematical transform is used to model the transform between plate coordinates from the two epochs. For this purpose we assume the mean proper motion over the considered field to be null or constant. This assumption is valid as long as there is no star streaming in any part of the field. The mathematical functions used are Legendre polynomial expansions.

$$X(x,y)=\sum a_{i,j}\,L_i(x)\,L_j(y)$$
$$Y(x,y)=\sum b_{i,j}\,L_i(x)\,L_j(y),$$

where L_i is a Legendre polynomial of order i, x, and y are the plate coordinates of about 2000 stars over $50\,cm^2$, the $a_{i,j}$ and $b_{i,j}$ are coefficients to be determined, X and Y are the transformed coordinates in the reference system of the other plate. Legendre polynomials do provide an orthogonal basis for the representation of functions on a rectangular window. It is not strictly true for the subspace represented by stars although they provide a reasonable approximation to orthogonality so far as stars involved in the transform are densely and uniformly distributed throughout the rectangular window.

Proper motions are given by:

$$\mu_x = x_{\text{Epoch 2}} - X(x_{\text{Epoch 1}}, y_{\text{Epoch 1}})$$
$$\mu_y = y_{\text{Epoch 2}} - Y(x_{\text{Epoch 1}}, y_{\text{Epoch 1}}).$$

Coefficients of X and Y transforms are estimated to minimize the rms proper motions. The 2000 selected stars (used to compute the mathematical transform) have been chosen after rejection of stars with large proper motion (15 μm), of stars that have been improperly centered at least one time and of the faintest stars.

The large number of stars allows the computation of transforms with high order polynomials and the correction of plate distortions at any scale length. Order 3 or 4 for the L_i (respectively 16 or 25 $a_{i,j}$ or $b_{i,j}$ coefficients) gives the best fit with a proper motions rms of 5 μm.

Figures 11 a, b give a representation of the X and Y order 4 transforms (only orders larger than 1 are represented). The coefficients of the transforms are given in the Table 5, the corresponding standard errors indicate the significance of the coefficients. Additional solutions based on subsets including only one half of the reference stars randomly chosen have been tried to check for the significance of the transform. Differences between two such solutions are plotted in Fig. 12; a reasonable agreement is obtained except near the border, it implies very few stars. This

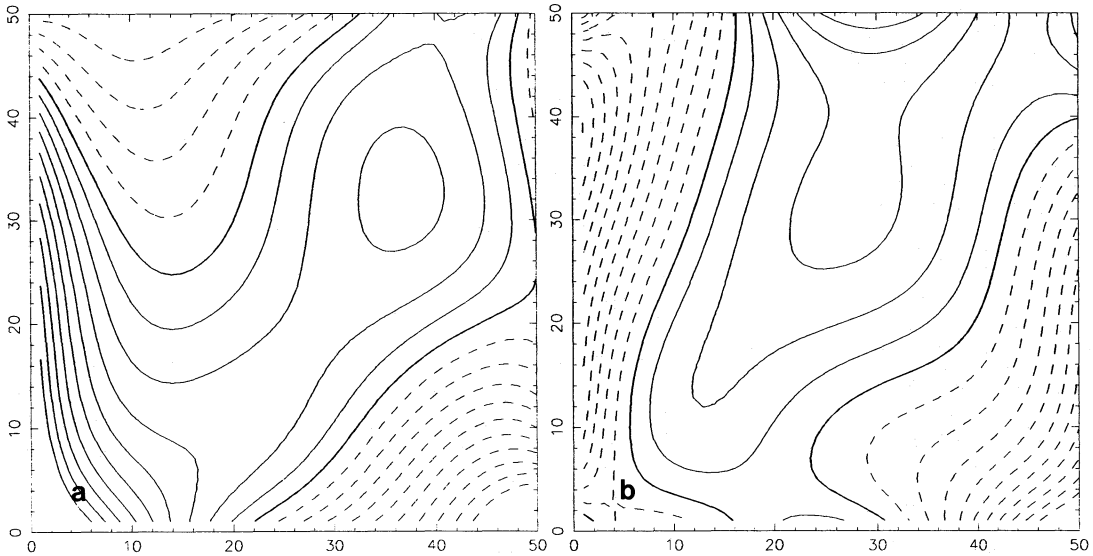

Fig. 11 a and b. Isocontour plot of the plate-plate transforms between CERGA plate 1523 and POSS copy 1402 over the analyzed area (about 64 cm^2). Constant and linear terms are ignored, the distance between isocontours is 1 μm, the thick line gives the zero level. **a** 4th order X transform on left panel. **b** 4th order Y transform on right panel

Table 5. Estimated coefficients of transforms $X(x, y)$ (col. 3) and $Y(x, y)$ (col. 4) at order 4. Indices i and j (cols. 1, 2) refer to the order in x and y respectively. Standard errors are given in column 5 (correlations are not given). The units are in μm

i	j	a_{ij}	b_{ij}	Error
0	0	55.9	−117.4	0.3
1	0	38323.1	−129.7	0.4
2	0	3.0	3.2	0.8
3	0	4.4	−2.0	0.8
4	0	−4.8	2.2	1.4
0	1	139.7	36763.2	0.4
0	2	2.6	1.4	0.8
0	3	0.2	−1.5	0.7
0	4	−1.3	0.2	1.5
1	1	−8.4	−5.7	0.6
1	2	4.3	0.3	1.3
1	3	−0.3	1.1	1.2
1	4	−1.5	−1.5	2.4
2	1	−2.6	5.2	1.3
2	2	4.2	−3.2	2.8
2	3	1.7	−3.9	2.4
2	4	−8.7	9.9	4.9
3	1	3.9	0.4	1.2
3	2	−3.1	−2.5	2.4
3	3	−3.0	−0.5	2.3
3	4	2.3	7.5	4.5
4	1	4.5	−5.6	2.3
4	2	−2.6	0.7	4.8
4	3	−2.6	2.4	4.4
4	4	9.4	−11.7	8.7

comparison indicates that the fourth order transforms are significant at the 0.5 μm accuracy level.

High orders (up to 10 corresponding to 121 coefficients) have been tried but the fit is not significantly improved, and the computed proper motions are only slightly modified. Differences between order 4 and 7 X and Y transforms are shown in Figs. 13a, b. The histogram of differences between μ_Y proper motions obtained from these two transforms is plotted in Fig. 14: the average change between orders 4 and 7 on proper motions is 0.5 μm in the Y transform but 1.0 μm in the X transform (largest changes remain near the borders where the transforms are loosely constrained). Figure 15 shows a plot of the difference between two 7th order transforms computed with two randomly selected subsamples. These two 7th order transforms are expected to model the same plate-plate transform but large deviations are observed (Fig. 15) and show that transforms are inaccurately defined.

In conclusion plate distortions can be modelled with 4th order X, Y transforms with an average accuracy of 0.5 μm without adding sizeable systematic errors. Higher order transforms will not improve the transform (i.e. distortions with scale lengths smaller than about 1 cm on plate cannot be modelled). Finally, as can be seen in Figs. 13a, b, transforms are poorly defined on the edges of the field.

Preliminary solutions have been tried using strictly orthogonal polynomials in which the coefficients a_{ij} and b_{ij} do not depend on the order of the expansion. Such exactly orthogonal polynomials combined with the stepwise regression method described by Hirte et al. (1990) are expected to allow a more rigorous error analysis.

4.2.3. Colour and magnitude terms

The whole star catalogue has been separated in three samples with different magnitude ranges ($V < 16.5$, $16.5 < V < 17.5$, $V > 17.5$). Transforms obtained in each magnitude range do not deviate from the reference one by more than a constant and a 0.5 μm rms spread. The constant is related to the kinematic differences of the considered sample of stars.

Similar comparisons have been performed also using two samples with different $B-V$ indices (smaller and greater than 0.7). Here again the accuracy of transforms is about 0.5 μm. Such tests are able to detect differential effects but are not suitable to reveal a magnitude or colour systematic bias in measured proper motions that would be constant over the field and could not be discriminated from the intrinsic magnitude or colour dependence of true proper motions.

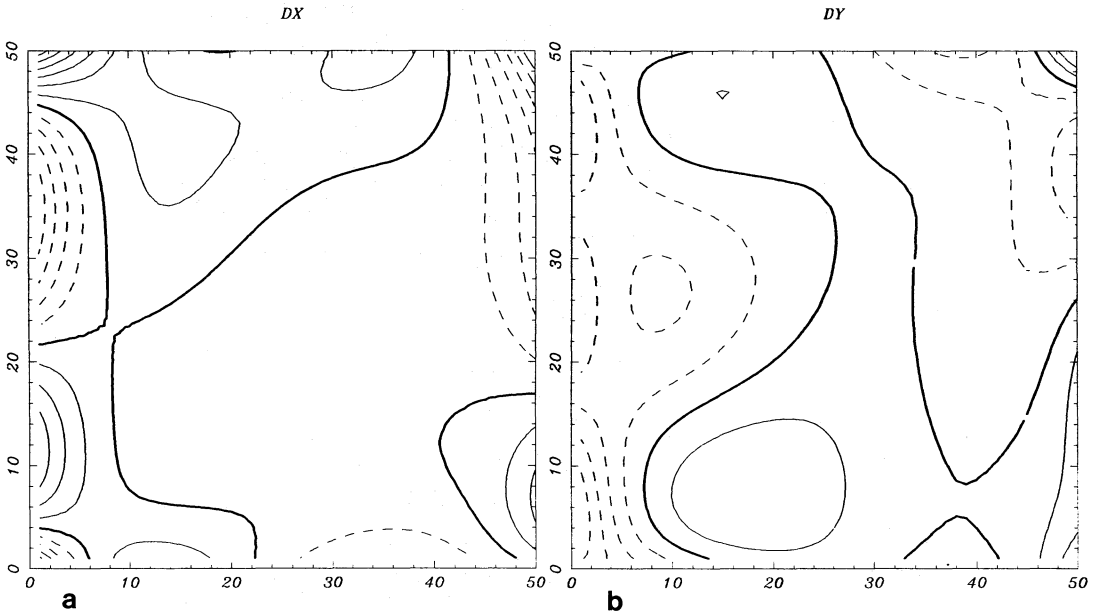

Fig. 12a and b. Isocontour plot differences between two 4th order transforms. The two transforms are determined with two independant subsets of stars, and they define identical transforms within better than ± 1 μm over most of the field. Differences give the amount of error in the transforms. The distance between isocontours is 1 μm. Thick line gives the zero level. **a** 4th order X transform on left panel. **b** 4th order Y transform on right panel

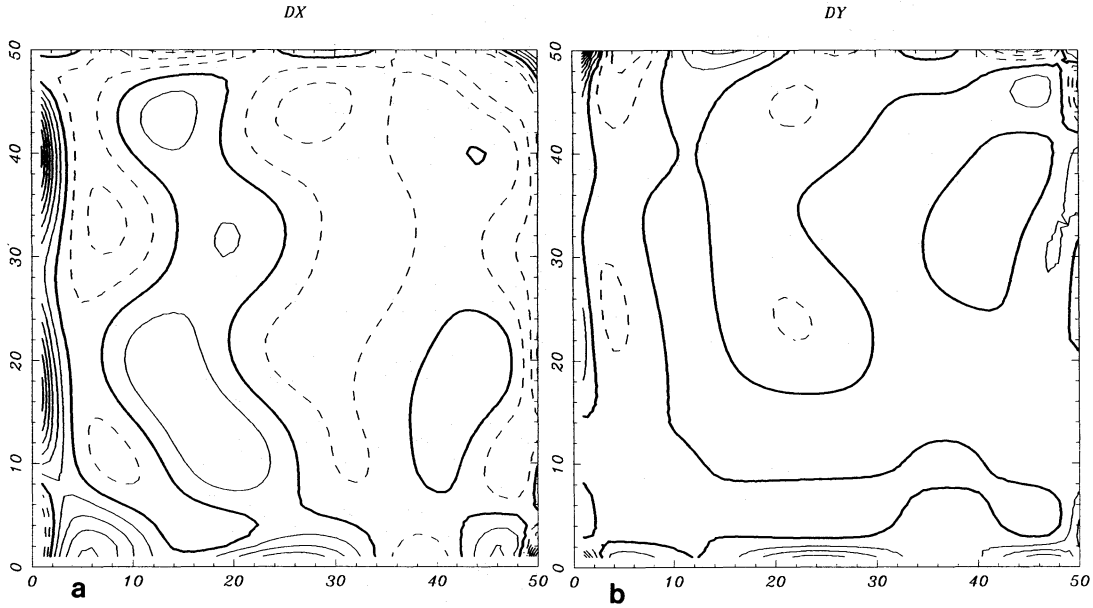

Fig. 13a and b. Differences between 4th and 7th order X and Y transforms. The thick line gives the zero level and step between lines is 1 μm. Strong differences are visible near the borders and are probably due to bad modelling with the order 7 and not due to existing distortions. **a** X transforms on left panel. **b** Y transforms on right panel

4.2.4. Overall error budget

The purely differential approach brings the following advantages already noted by Chiu (1980): (1) we avoid determining and modelling the plate constants, (2) the solution does not depend on the accuracy of celestial coordinates of any intermediate catalogue, (3) the exact accuracy of the reference system only depends on the number of stars and on the rms proper motions, (4) it is possible to measure proper motions using plates from different instruments, even glass copies and different plate centers.

The overall proper motion accuracy can be deduced from the various sources of errors. Sources of random errors are the plate noise, the digitizing machine, the centering algorithms, the plate-plate transforms. In the present catalogue the main source of error is the plate noise corresponding to about 0.8 μm on bright star proper motions (Sect. 4.1), other contributions are smaller or equal to 0.5 μm (Sect. 4.2). Then the global errors are definitely less than 3 mas yr^{-1} for bright stars ($V < 16$) and about 6 mas yr^{-1} for the faintest ($V = 17.5$). With such an accuracy, known systematic errors must be considered carefully: we have shown that colour effects and magnitude effects are small. Since we have used only one first epoch plate, we were not able to check for a magnitude effect on the POSS copy. From our experience and since stellar images were round enough on that plate, a magnitude effect is not likely to exceed 1 μm. Only measuring the second POSS plate of this field would give a definite answer.

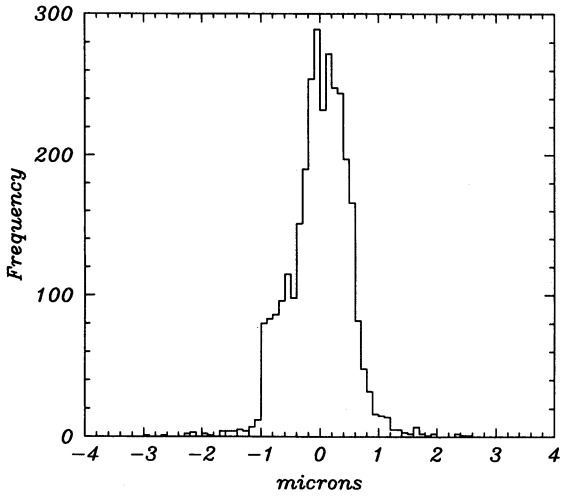

Fig. 14. Histogram of the differences between delta proper motions based on 4th and 7th order Y transforms determined using all the stars of our catalogue. This allows to estimate the robustness of the modelling transformations. The average rms on differences is 0.5 μm

The proper motions accuracy is comparable with the accuracy expected for the HIPPARCOS mission although only relative. The key conditions for such a performance are (1) an astrometric machine like the MAMA giving access to submicron accuracies, (2) the choice of the centering algorithms, gravity center methods (modified or not....) is not the best choice and would decrease the accuracy for faint stars, (3) plate-to-plate transforms using polynomial expansions allow the modelling of small scale distortions on plates: this method is restricted to fields with a sufficient star density and would fail in detecting local streaming motions. Further improvements are expected from using orthogonal polynomial expansions since they would allow an exact determination of the errors on transforms. In an investigation under progress more accurate astrometry (1.5 mas yr^{-1}) is obtained with 11 plates from three different Schmidt telescopes, this is probably the way to detect and avoid instrumental bias. In Sect. 5, the whole error analysis is validated by comparing the colour-proper motion distribution with predictions from a kinematic model. This comparison shows that errors have not been underestimated: much larger error would hide kinematics features which are clearly visible in the data.

4.2.5. Reduction to absolute proper motions

Correcting proper motions from differential to absolute should rely upon galaxies or bright astrometric standards, either kinds of objects are scarce in the field and unaccurately centered. Both possibilities have been explored giving compatible results although within error bars far larger than the differential ones so it does not provide much in terms of kinematic information. The best we can do in this context is to propose model dependent corrections. Such constants can be determined for instance from the kinematic version (Robin & Oblak 1987) of the Besançon model. To convert data to absolute proper motions, it is necessary to add to μ_l and μ_b respectively the constant $-0''.576$ and $0''.060$ $century^{-1}$.

5. Discussion

The catalogue in V, $B-V$, $U-B$, μ_l, μ_b resulting from the present work provides a five-dimensional probe of the stellar populations in the Milky Way.

A detailed investigation of the significance of these new data in terms of galactic structure and evolution will be published separately. Some preliminary results relevant to the thick disk population have been presented previously (Robin et al. 1989; Bienaymé et al. 1989). In the following we give a few comparisons of the distribution of observable quantities with model predictions in so far as such comparisons can help evaluating the performances of the data. Since there is no substantial overlap of the catalogue with any data of comparable accuracy, this is the only way to get an external assessment of the error budget.

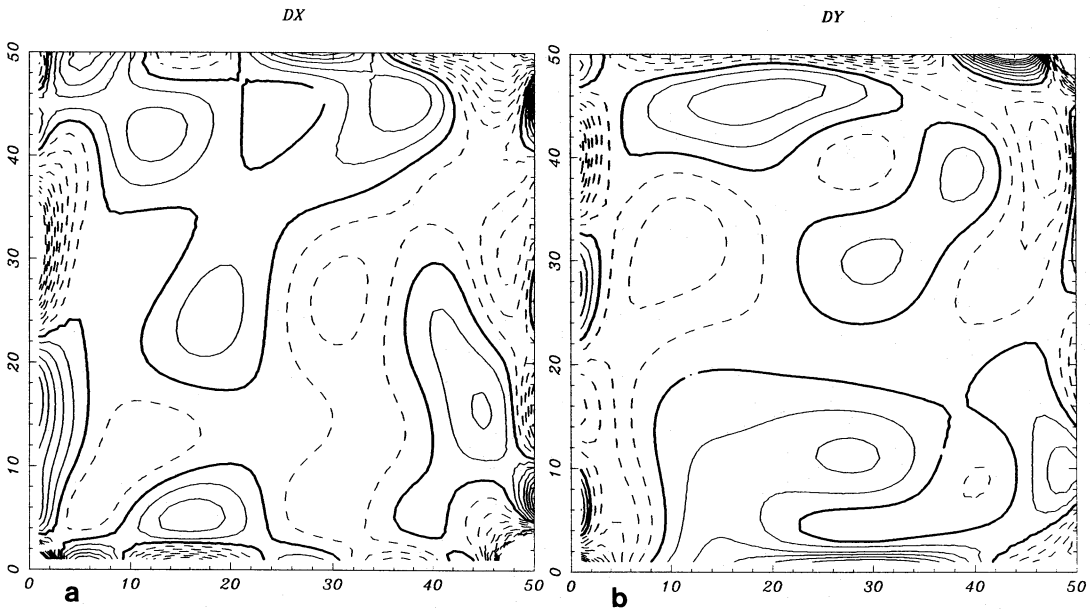

Fig. 15a and b. Same as Fig. 13 but with two 7th order transforms. Differences between the transforms are much bigger and illustrate that 7th order transforms are inaccurately determined. **a** X transforms on left panel. **b** Y transforms on right panel

The Besançon model does provide a suitable framework for such an assessment. The mainsprings of this polulation synthesis model are described in Robin & Crézé (1986) (star formation, stellar evolution, photometric predictions), Bienaymé et al. (1987) (dynamical consistency), Robin & Oblak (1987) (kinematic predictions). Being intrinsically based on a scenario relating the distribution of stars in the phase space to their age and evolutionary characteristics, this model can predict without additional empirical ingredients the multivariate distribution of astrometric and photometric observables. It is then appropriate to investigate how far predictions depend on the basic characteristics of the model and on the level of observational errors.

Histograms and diagrams of observed and model-predicted proper motions in three magnitude ranges are plotted in Figs. 16 and 17. The asymmetric shape of the distribution of longitudinal proper motions is clearly visible in both the data and model. According to the model, this asymmetry results from the asymmetric drift. Most stars contributing to the histograms are found a few hundred parsecs away from the Sun, at this distance the stellar drift is reflected in proper motions by roughly 1 arcsec per century. The standard error of proper motions has been set to 0".3 per century in the model, as a result of the above analysis of the astrometric accuracy. In case the error analysis were grossly wrong, the asymmetric drift effect would disappear as can be seen in Figs. 18a, b. In the same way, in Fig. 18c, model velocity dispersions have been arbitrarily increased by factor 1.5. Larger velocity dispersions althouth resulting in an increase of the dispersion of proper motions, leaves the signature of the asymmetric drift unaltered. So the quality of the astrometric data alone allows the accurate measurement of important kinematic features.

Combined astrometric and photometric data provide multivariate constraints to the model which cannot be visualized in any simple projection diagram. In order to illustrate the power of such

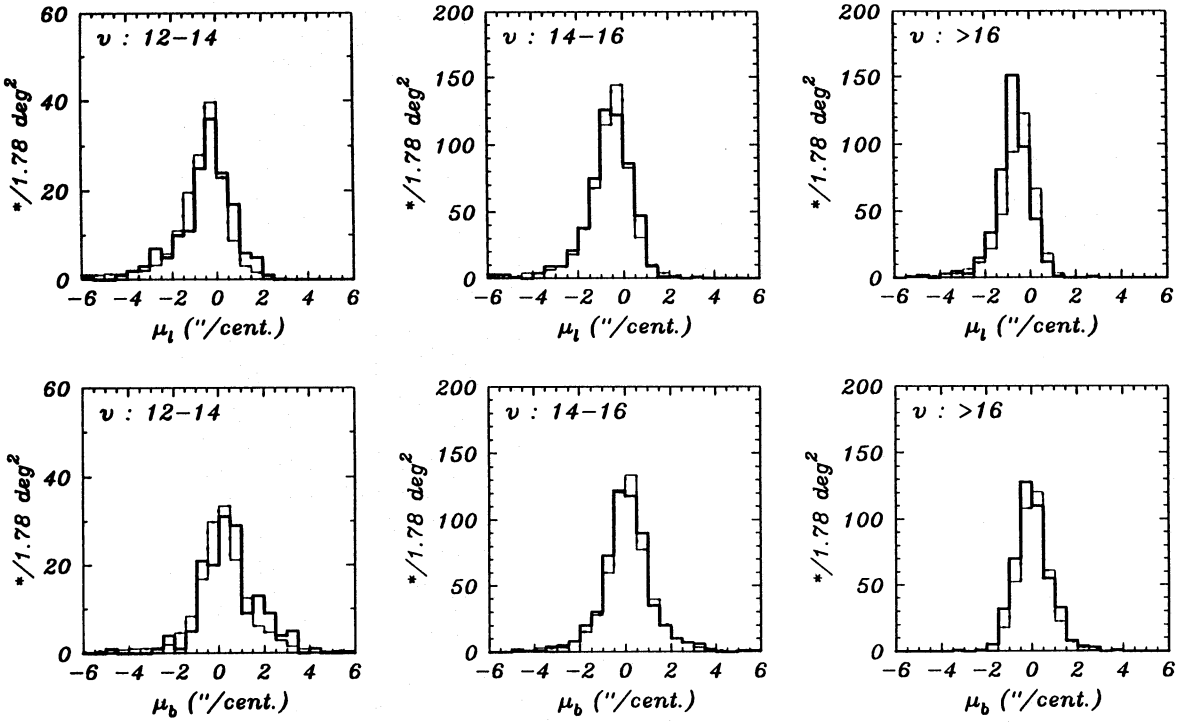

Fig. 16. μ_l and μ_b observed proper motion histograms for three v instrumental magnitude intervals. Data (solid lines) and model prediction (thin dotted lines)

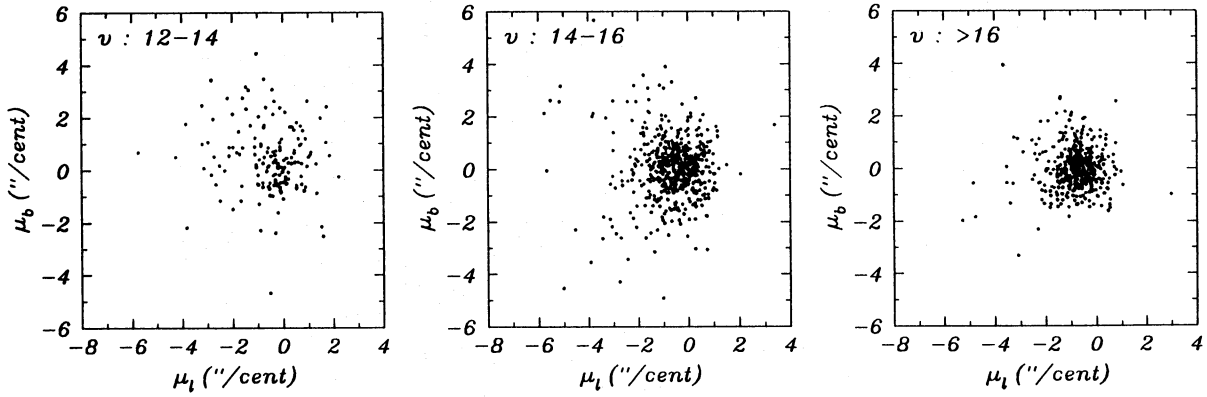

Fig. 17. μ_l and μ_b proper motion diagrams for three v instrumental magnitude intervals

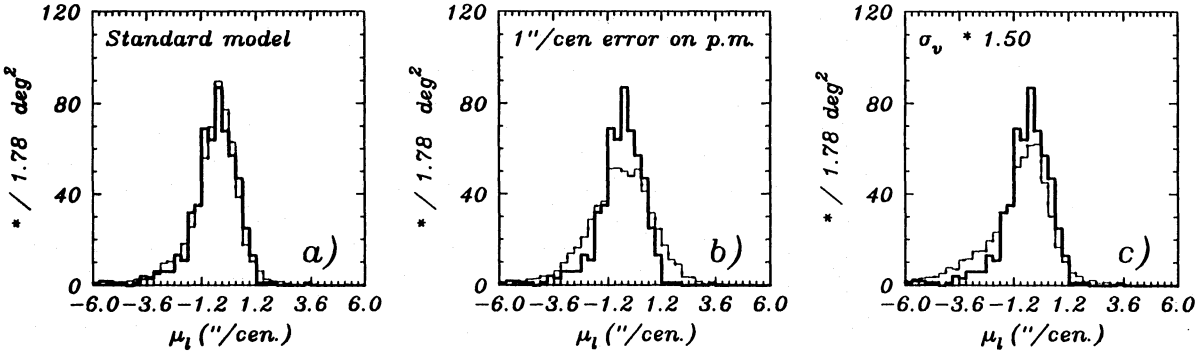

Fig. 18a–c. μ_l proper motion histograms for stars with $14 < v < 16$. Data (solid lines) can be compared to model predictions (thin dotted lines). **a** Standard model with an assumed 0".3 century^{-1} accuracy on proper motions, **b** with an assumed 1".0 century^{-1} accuracy on proper motions, **c** as **a** but velocity dispersion of stars is increased by 50%

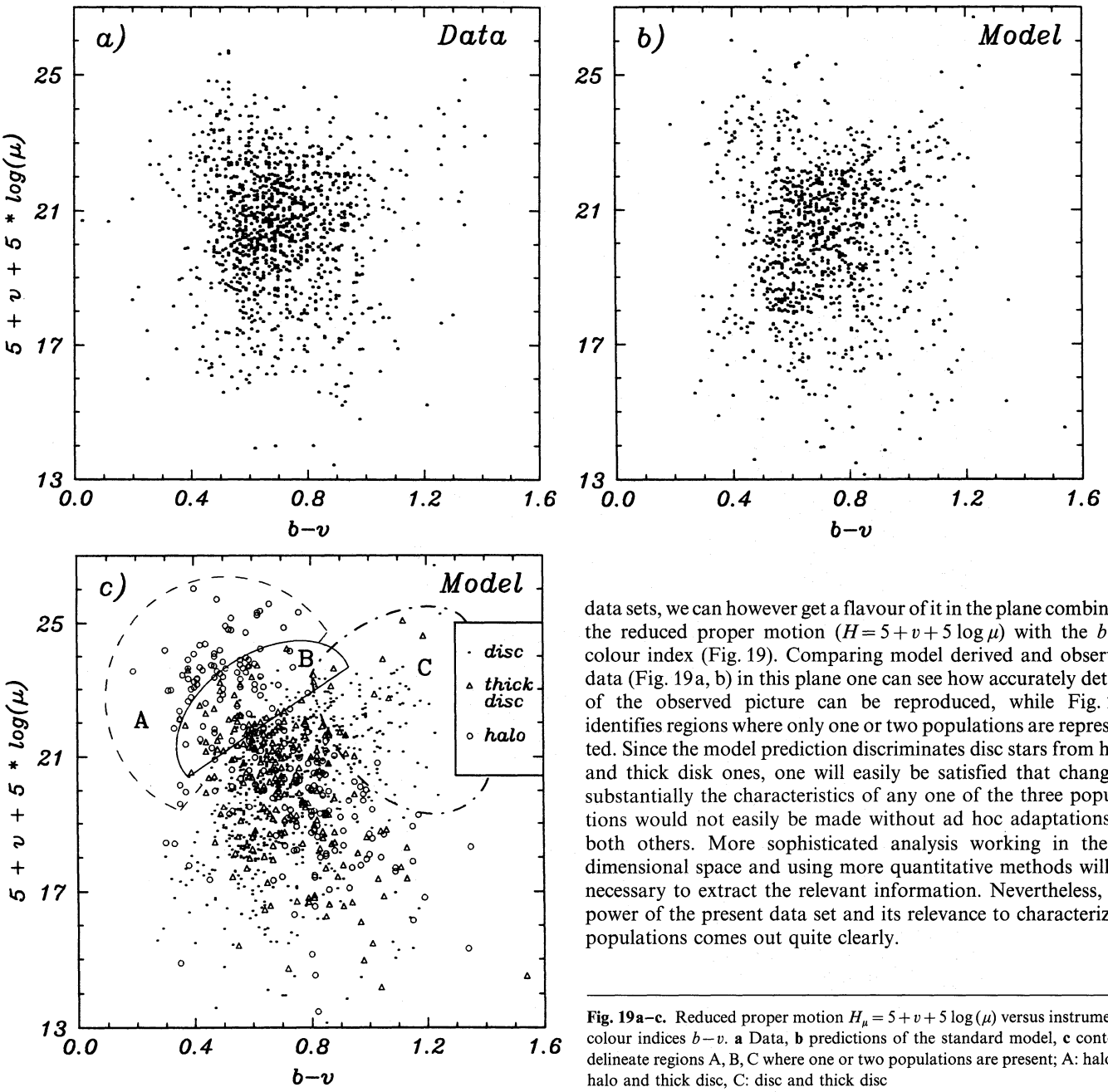

data sets, we can however get a flavour of it in the plane combining the reduced proper motion ($H = 5 + v + 5 \log \mu$) with the $b-v$ colour index (Fig. 19). Comparing model derived and observed data (Fig. 19a, b) in this plane one can see how accurately details of the observed picture can be reproduced, while Fig. 19c identifies regions where only one or two populations are represented. Since the model prediction discriminates disc stars from halo and thick disk ones, one will easily be satisfied that changing substantially the characteristics of any one of the three populations would not easily be made without ad hoc adaptations of both others. More sophisticated analysis working in the 5-dimensional space and using more quantitative methods will be necessary to extract the relevant information. Nevertheless, the power of the present data set and its relevance to characterizing populations comes out quite clearly.

Fig. 19a–c. Reduced proper motion $H_\mu = 5 + v + 5 \log(\mu)$ versus instrumental colour indices $b-v$. **a** Data, **b** predictions of the standard model, **c** contours delineate regions A, B, C where one or two populations are present; A: halo, B: halo and thick disc, C: disc and thick disc

Appendix A

Available data for photometric calibrations are given in Table A1 and come from:

(1) Photoelectric observations

Authors	Identification
Arp (1962)	A–U
Mohan (1987)	a–z

(2) CCD observations

Authors	Identification	
Richer & Fahlman (1987)	Middle field Outer field	R1–R8 R11–R13
Stetson & Harris (1988)		S1–S55
Mohan (1987)	Field I	1–21
Mohan et al. (1991)	Field I Field II	Y1–Y37 C1–C7

Table A1

Identification	*V*	*B*	*U*	α 1950	δ 1950
w	11.13*	12.20	13.11	$15^h10^m21^s.54$	2°47′58″.8
p	11.26*	12.84	14.74	15 13 48.16	2 55 51.5
z	11.12*	11.25*	11.41*	15 11 59.25	2 54 58.2
j	11.48*	12.39	12.87	15 9 57.23	1 55 7.2
o	11.45*	11.92*	11.91*	15 13 39.96	2 51 40.4
l	11.87	13.17	14.69	15 15 18.49	2 23 48.3
t	11.79	12.47	12.66	15 9 40.75	2 28 8.6
x	11.94	12.42	12.39	15 12 8.31	2 48 18.5
m	12.04	12.61	12.68	15 15 3.16	2 36 23.4
u	12.09	12.83	13.14	15 10 28.45	2 34 1.1
s	12.10	12.84	13.12	15 10 11.56	2 27 16.4
g	12.22	12.73	12.75	15 10 1.92	1 30 57.8
D	12.35	13.50	14.62	15 15 22.32	2 14 31.8
d	12.40	13.38	14.24	15 14 38.62	1 39 13.9
y	12.42	13.42	14.04	15 9 53.53	2 53 49.4
f	12.38*	12.99*	13.15*	15 14 35.85	1 52 12.1
E	12.38	12.98	13.09	15 15 22.63	2 17 8.9
15	12.43	13.04	13.16	15 15 22.63	2 17 8.9
k	12.48	13.38	13.90	15 9 54.72	2 5 13.6
v	12.54	13.39	13.86	15 11 23.59	2 44 16.6
e	12.52	13.03	13.02	15 15 14.22	2 0 13.8
r	12.71	13.94	14.91	15 9 53.16	2 14 30.8
b	12.65	13.25	13.28	15 13 4.52	1 31 0.7
h	12.81	13.39	13.49	15 11 27.20	1 36 7.6
q	12.90	13.77	13.95	15 14 40.15	2 56 8.9
i	13.01	14.01	14.70	15 9 55.42	1 46 27.3
S51	13.19	14.38*		15 15 32.38	2 16 47.1
c	13.39	14.08	14.26	15 14 41.47	1 31 55.5
n	13.48	14.27	14.62	15 15 15.16	2 49 11.4
Y1	13.90	14.95	15.69	15 15 27.27	2 17 14.7
a	13.99	14.89	15.68	$15^h12^m29^s.16$	1°30′59″.3
G	14.37	15.32	15.98	15 16 2.63	2 7 9.1
Y2	14.59	15.51	16.05	15 15 23.60	2 18 16.1
Y3	14.64	15.15	14.94	15 15 21.71	2 17 50.9
S55	14.80	15.69		15 15 32.87	2 16 34.3
11	14.95	15.51	15.52	15 15 28.71	2 18 0.3
18	15.04	15.54	15.51	15 15 25.49	2 18 51.5
19	15.03*	15.15	15.05*	15 15 21.44	2 18 49.3
C1	15.16	16.15	17.02	15 9 49.83	1 36 58.8
12	15.12	15.57	15.74	15 15 33.17	2 17 55.9
8	15.72	16.70	16.81*	15 15 28.62	2 17 5.0
H	15.69	15.61	15.44	15 15 32.45	2 14 28.3
S2	15.92	16.74		15 15 19.42	2 16 30.3
I	15.96	16.70	16.98	15 15 15.26	2 14 16.8
C2	16.12	17.21	18.34*	15 9 52.83	1 36 16.2
C3	16.39	17.24	17.50	15 9 40.64	1 37 4.7
R13	16.42	17.03	17.09	15 14 18.78	2 17 9.3
J	16.61	17.31	17.43*	15 15 24.48	2 14 18.7
K	16.67	17.66		15 15 25.68	2 13 50.6
L	16.70	17.50	17.69	15 15 16.65	2 15 45.3
R11	16.79*	17.51	17.76	15 14 12.68	2 17 10.3
S44	16.80	17.57		15 15 31.87	2 16 16.8
M	17.00	17.70		15 15 22.43	2 13 15.3
N	17.25	18.36	19.12*	15 15 24.39	2 16 42.5
O	17.26	17.96	18.13	15 15 25.51	2 14 52.0
S24	17.27	17.99		$15^h15^m28^s.15$	2°16′26″.7
S15	17.36	18.44*		15 15 24.39	2 16 42.5
20	17.32	18.07	18.53*	15 15 26.90	2 18 58.4
R8	17.52	18.81*		15 15 28.04	2 19 37.0
P	17.57	18.24	18.42*	15 15 24.55	2 18 42.4
Y10	17.59	18.30	18.24	15 15 24.55	2 18 42.4
S1	17.60	18.32		15 15 18.47	2 16 15.9
Q	17.58	18.16		15 15 19.05	2 18 55.1
R	17.65	18.25		15 15 19.35	2 15 32.3
S47	17.70*	18.37*		15 15 32.02	2 15 55.4
R12	17.82*	19.35*		15 14 15.83	2 15 21.2
S6	17.76*	18.47*		15 15 21.49	2 16 22.2
S53	17.91*	19.43*		15 15 32.73	2 16 22.4
Y16	17.95*	18.53*	18.33	15 15 29.22	2 17 25.6
S14	18.00*	18.61*		15 15 23.53	2 16 43.6
Y13	18.00*	18.55*	18.38*	15 15 31.28	2 17 30.7
Y18	18.04*	18.61*	18.40*	15 15 27.20	2 17 5.1
S39	18.06*	18.59*		15 15 31.19	2 16 15.4
S29	18.07*	18.57*		15 15 28.96	2 16 14.8
S49	18.12*	18.64*		15 15 32.30	2 15 34.9
S4	18.25*	18.76*		15 15 20.39	2 16 29.1
Y19	18.25*	18.76*	18.60*	15 15 27.75	2 18 54.3
Y20	18.26*	18.76*	18.62*	15 15 20.50	2 18 33.7
S5	18.27*	18.75*		15 15 20.44	2 16 12.8
S8	18.29*	18.78*		15 15 22.33	2 16 35.9
C5	18.34*	18.80*	18.37*	15 9 50.38	1 36 14.7
R1	18.48*	19.87*		15 15 20.69	2 17 39.7
S32	18.36*	18.87*		15 15 30.06	2 15 21.7
Y24	18.51*	19.96*		15 15 20.69	2 17 39.7
S45	18.38*	18.85*		15 15 31.99	2 16 25.1
S40	18.41*	18.88*		15 15 31.29	2 16 30.2
Y23	18.46*	18.98*	18.69*	15 15 21.99	2 17 32.6

Table A1 (continued)

Identification	V	B	U	α1950	δ1950
T	18.53*	18.98*	18.84*	$15^h15^m20^s27$	2°15′48″9
S22	18.54*	19.02*		15 15 27.79	2 15 21.8
S3	18.56*	19.01*		15 15 20.27	2 15 49.0
R4	18.65*	19.12*		15 15 25.23	2 18 4.1
Y26	18.67*	19.19*	18.93*	15 15 30.55	2 17 42.8
S36	18.68*	19.15*		15 15 30.46	2 16 20.9
Y28	18.68*	19.14*	19.04*	15 15 31.82	2 17 44.6
Y29	18.69*	19.16*	18.84*	15 15 25.23	2 18 4.1
V	18.72*	19.29*	19.34*	15 15 19.60	2 13 33.2
C7	18.84*	20.23*		15 9 42.63	1 36 1.6
S37	18.76*	19.22*		15 15 30.57	2 15 53.2
R7	18.77*	19.23*		15 15 21.33	2 18 37.7
Y31	18.77*	19.26*	19.04*	15 15 30.31	2 18 30.4
C6	18.77*	19.22*	18.95*	15 9 53.32	1 37 51.1
S33	18.81*	19.29*		15 15 30.18	2 16 8.4
Y33	18.86*	19.34*	18.99*	15 15 28.76	2 18 36.4
Y36	18.88*	19.37*	19.09*	15 15 22.15	2 18 34.4
S9	18.88*	19.36*		15 15 22.33	2 16 53.7
Y34	18.90*	19.41*	19.11*	15 15 22.33	2 16 53.7
S25	18.90*	19.42*		15 15 28.17	2 16 37.4
R6	18.91*	19.36*		15 15 22.15	2 18 34.4
S38	18.97*	19.49*		15 15 30.60	2 15 49.1
Y37	18.98*	19.47*		15 15 31.96	2 18 11.8

Stars not used in our photographic calibration are labelled with *

Coordinates (equinox 1950) are obtained from our catalogue. Magnitudes are given in the Johnson system.

Stars f, S 51, 19 (and star 8 for U magnitude) have been rejected from the photographic calibration process on the basis of high residuals in preliminary solutions.

Our calibration curves are not defined outside the following intervals $11.4 < v < 17.5$; $12 < b < 18.5$; $12.25 < u < 18.6$, where u, b, and v are instrumental magnitudes.

Acknowledgements. We thank M. Chareton for his help with data reduction. We would like to thank Dr. R. Le Poole and Dr. J. Guibert for helpful discussion during the course of this investigation. We are particularly indebted to the Leiden Observatory that let us the possibility to scan plates from its POSS collection. Finally we thank all the CAI/MAMA and CERGA Schmidt staffs who made this investigation possible.

References

Arp H., 1962, ApJ 135, 311
Becker W., 1965, Z. Astrophys. 62, 54
Berger J., Cordoni J.P., Fringant A.M., Guibert J., Moreau O., Reboul H., Vanderriest C., 1991, A&AS 87, 389
Bienaymé O., Robin A.C., Crézé M., 1987, A&A 180, 94
Bienaymé O., Mohan V., Crézé M., Considère S., Robin A.C., 1989, The gravitational force perpendicular to the galactic plane. Philip A.G.D., Lu P.K. (eds.) Proc. of a Conference held at Danbury. Davis Press, Schenectady, N.Y., p. 53
Bienaymé O., Motch C., Crézé M., Considère S., 1988, Symp. IAU 133, Mapping the sky. Debarbat S. et al. (eds.) Kluwer, London, p. 389
Bok B.J., Basinski J., 1964, Mem. Mount Stromlo Observatory vol. 4, 1, No. 16
Chiu L.T.G., 1980, ApJS 44, 31
Fenkart R., Karaali S., 1990, A&AS 83, 481
Gilmore G., Wyse R.F.G., 1985, AJ 90, 2015
Hirte S., Dick W.R., Shilbach E., Scholz R., 1990, Errors, bias and uncertainties in astronomy. Jaschek C., Murtagh F. (eds.) Cambridge University, Cambridge, p. 343
Kovalevsky J., 1990, Lecture notes in Physics, Astrométrie moderne. Springer, Berlin Heidelberg New York, p. 49
McCuskey S.W., 1965, Stars and Stellar Systems, vol. V. Galactic Structure. Blaauw A., Schmidt M. (eds.) University of Chicago, Chicago, p. 1
Mohan V., 1987, Thesis. University of Nice
Mohan V., Robin A.C., Crézé M., 1991 (private communication)
Mohan V., Crézé M., 1987, A&AS 68, 529
Murray C.A., Corben P.M., 1979, MNRAS 187, 723
Reid N., 1990, MNRAS 247, 70
Richer H.B., Fahlman G.G., 1987, ApJ 316, 189
Robin A.C., Crézé M., 1986, A&A 157, 71
Robin A.C., Crézé M., Bienaymé O., Oblak E., 1989, The Gravitational Force Perpendicular to the Galactic Plane. Philip A.G.D., Lu P.K. (eds.) Proc. of a Conference held at Danbury. David Press, Schenectady, N.Y., p. 33
Robin A.C., Oblak E., 1987, Publ. Astron. Inst. Czech. Acad. Sci. 69, 323
Sandage A., 1987, AJ 93, 610
Spaenhauer A., 1989, The Gravitational Force Perpendicular to the Galactic Plane. Philip A.G.D., Lu P.K. (eds.) Proc of a Conference held at Danbury. David Press, Schenectady, N.Y., p. 45
Stetson P.B., Harris W.E., 1988, AJ 96, 909
Stone R.C., 1989, AJ 97, 1227
van Rhijn P.J., 1965, Stars and Stellar Systems, vol. V. Galactic Structure. Blaauw A., Schmidt M., (eds.) University of Chicago, Chicago, p. 27
Yoshii Y., Ishida K., Stobie R.S., 1987, AJ 92, 323